Solid Freeform Fabrication 2017: Proceedings of the 28th Annual International Solid Freeform Fabrication Symposium – An Additive Manufacturing Conference
Reviewed Paper

MODELLING NANOPARTICLE SINTERING IN A MICROSCALE SELECTIVE LASER SINTERING PROCESS

Obehi G Dibua*, Nilabh K Roy*, Anil Yuksel**, Chee S Foong†, Michael Cullinan*

*Department of Mechanical Engineering, University of Texas at Austin, Austin, TX 78712
**Institute for Computational Engineering and Sciences, University of Texas at Austin, Austin, TX 78712
†NXP Semiconductors, Austin, TX 78735

Abstract

An important aspect of making microscale selective laser sintering (μ-SLS) a viable commercial process is having the ability to predict the structural properties of sintered parts. This prediction is made possible through accurate models of the sintering process. The majority of SLS models simulate sintering as a melting process which is accurate for microparticles. However, for nanoscale particles the sintering process becomes dominated by grain boundary and surface diffusion between particles. Though there are currently research efforts on modeling the sintering behavior between nanoparticles, these efforts revolve around simulations with only a few particles. This paper presents an approach to modelling diffusion between nanoparticles in full sized beds made up of hundreds of particles. The simulations presented in this paper are done using a phase field modeling (PFM) approach that can be used to predict properties such as the porosity, shrinkage and relative density of sintered parts, which can then be compared against experimental data.

Introduction

Common additive manufacturing (AM) processes are typically only able to produce parts with ~100μm resolution [1,2]. As such, the desire for microscale parts with nanoscale resolution has prevented AM technologies from advancing into industries where small feature sizes are critical such as the microelectronics industry. In the microelectronics industry, parts are typically made using a combination of lithography, etching and material deposition processes to create 2½D electronic structures. However, the complexity and size limitations on these processes gives rise to the need for a more flexible manufacturing process for matching the desired tolerances. One option for creating 3D microelectronic structures is microscale selective laser sintering (μ-SLS) of nanoparticles [3-5]. As this new technology rises, there is a concurrent need for models capable of predicting the properties of sintered parts.

Though there are a number of accurate SLS models [6-8], these models approximate sintering as a melting process. Due to the micron sizes of the particles used in SLS, the mass transfer taken place between particles is dominated by microscale effects like melting. When transitioning from the sintering of microscale to nanoscale particles the mechanism behind sintering changes. During the sintering of nanoparticles there are a number of processes taken place including, but not limited to, viscous flow, grain-boundary sliding/dislocations, volume, vapor, grain boundary and surface diffusion [9]. However, for the size of particles used in this study the dominant means of sintering has been shown to be surface and grain boundary diffusion

[9]. As such, the model discussed in this paper focusses mainly on surface and grain boundary diffusion and minimally on volume diffusion.

Background

There are currently a number of simulations studying diffusion as the prominent force driving the sintering of particles. Rojek et al, modelled sintering as a diffusion process using a discrete element method (DEM) [10]. They found that shrinkage between particles was driven by stresses and surface tension in the neck which attracted particles towards each other. Though this model uses a large number of particles, it models sintering as a bulk process governed by a particle interaction model dependent on only grain boundary diffusion. Ding and Pan have studied the sintering between nanoparticles using molecular dynamics which tracks the interaction between atoms in the particles [11]. This simulation made use of the Lennard-Jones model to track the potential between particles, tracking the kinetics of two and three particles at a time. Ding and Pan compared continuum and molecular dynamics (MD) models for modelling sintering between nanoparticles. They found that the preliminary assumptions required for continuum models made them inadequate for tracking the sintering kinetics which morphed during atomistic interactions in the MD models. Using MD simulations Cheng and Ngan were able to expand from the few particle simulations done by Ding and Pan to track four particles in an FCC crystalline state [12]. They found that at low temperatures the governing sintering mechanism was found to be a variety of plasticity processes including dislocation and twinning. The downside with these simulations is that the discrete models are unable to model nanoscale features and the molecular dynamics (MD) simulations are too computationally expensive to model full particle beds. Phase field modelling (PFM) offers the potential to overcome these limitations by enabling the modelling of nanoscale effects for large numbers of particles.

Phase field models have been created to track the sintering behavior between particles. Shinagawa used a combination of phase field modeling and the discrete-element method to track the sintering between a cluster made up of 10 particles [13]. Wang used PFM to track the sintering between 26 particles [14]. Both of these models however track the sintering of particles in 2D. 2D simulations, though they provide useful insight into the diffusion process, cannot be used to predict the results of a real particle bed such as volume shrinkage. Kumar used PFM to track the sintering of 28 3D particles randomly arranged in a cubic lattice [15]. In contrast to those previously developed models, the simulation used in this study is able to track the diffusion between hundreds of particles using phase field modeling. Taking advantage of the computational advances made possible through parallel computing, this study simulates the behavior of sintering particles in a real particle bed and results are shown for a one-by-one micron bed containing 43 particles and a two-by-two micron bed containing 134 particles. A data analysis package was also created which gives the change in density and height of the particles in the simulation. From this analysis, the density of the powder bed as a function of simulation time is determined which can be compared against similar results from experimental measurements on real powder beds.

Model

Phase field modelling is a diffuse-interface approach which tracks the evolution of particles using phase field variables related to microscopic parameters [16]. The model used in this study

makes use of mass density (ρ) and the order parameter (η_i) as the phase field variables. Both of these variables take on values from 0 to 1. The density variable takes the value of 1 when in a solid phase, 0 when in vapor and values between 0 and 1 at the interphases. The order parameter on the other hand is unique for each particle, taking on the value of 1 for the ith particle and 0 everywhere else. The evolution of these variables is driven by the minimization of the total free energy in the system. The free energy is a function of the phase-field variables and is given in Eq. 1.

$$F = \int_V \left[f(\rho, \eta_i) + \frac{1}{2}\beta_\rho |\nabla \rho|^2 + \frac{1}{2}\sum_{i=1}^{N} \beta_\eta |\nabla \eta_i|^2 \right] dV \tag{1}$$

where $f(\rho, \eta_i)$ is the bulk free energy, N is the total number of particles in the system, β_ρ is the gradient energy term for the density variable, and β_η is the gradient energy term for the order parameter. Both gradient energy terms are related to the surface and grain boundary energies of the system. The bulk free energy is a Landau type potential with the form in [15] adopted here, and is shown in Eq. 2.

$$\begin{aligned} f(\rho, \eta_i) = \; & K_1 \left(\rho^4 + \frac{-4\rho_{vap} - 4\rho_{sol} - 2}{3}\rho^3 + \frac{4\rho_{vap}\rho_{sol} + 2\rho_{vap} + 2\rho_{sol}}{2}\rho^2 - 2\rho_{vap}\rho_{sol}\rho \right) \\ & + K_2 \left(\rho^2 + 6(1-\rho)\sum_{i=1}^{N} {\eta_i}^2 - 4(2-\rho)\sum_{i=1}^{N} {\eta_i}^3 + 3\sum_{i=1}^{N} {\eta_i}^4 \right. \\ & \left. + w\sum_{i=1}^{N}\sum_{j=1, j\neq i}^{N} {\eta_i}^2 {\eta_j}^2 \right) \end{aligned} \tag{2}$$

where ρ_{vap} and ρ_{sol} are the vapor and solid density parameters respectively and w is related to the grain boundary energy. Chockalingam et al [17], showed that K_2 in Eq. 2 and β_η in Eq. 1 are related to the grain boundary energy by Eq. 3, and K_1, K_2, β_ρ and β_η are related to the surface energy of the particles in the system by Eq. 4. Where γ_{gb} in Eq. 3 is the grain boundary energy and γ_s in Eq. 4 is the surface energy.

$$\gamma_{gb} = \frac{2\sqrt{K_2 \beta_\eta}}{\sqrt{3}} \tag{3}$$

$$\gamma_s = \frac{\sqrt{2(\beta_\rho + \beta_\eta)(K_1 + 7K_2)}}{6} \tag{4}$$

The temporal evolution of the density field variable is governed by the Cahn-Hilliard equation [18,19] shown in Eq. 5.

$$\frac{\partial \rho}{\partial t} = \nabla . \left(D \nabla \frac{\delta F}{\delta \rho} \right) = \nabla . \left(D \nabla \left[\frac{\partial f(\rho, \eta_i)}{\partial \rho} - \beta_\rho \nabla^2 \rho \right] \right) \tag{5}$$

where D is the equivalent diffusion coefficient made up of fractions of the surface, grain boundary and volume diffusion coefficients. The equivalent diffusion coefficient is given in Eq. 6.

$$D = D_{vol}\emptyset + D_{surf}\rho^2(1-\rho^2) + D_{gb}\rho\left(1 - \sum_{i=1}^{N} {\eta_i}^2\right) \quad (6)$$

where D_{vol}, D_{surf}, D_{gb}, are the volume, surface and grain boundary diffusion coefficients respectively, and $\emptyset = \rho^4(7\rho^2 - 18\rho + 12)$ having a maximum in the solid phase and a minimum in the vapor phase [15].

The temporal evolution of the order parameter is governed by the time-dependent Ginzburg-Landau structural relaxation equation [20] given in Eq. 7.

$$\frac{\partial \eta_i}{\partial t} = -L\frac{\partial F}{\partial \eta_i} = -L\left(\frac{\partial f}{\partial \eta_i} - \beta_\eta \nabla^2 \eta_i\right) \quad (7)$$

where L is a constant that characterizes grain boundary mobility.

Simulation

The equations above where discretized using the Forward Euler method for numerical differentiation. The simulation was developed into a C++ code and run with units of simulation time steps and pixel length. The Message Passing Interface (MPI) was used to break the simulation box up into different portions that could be solved with different processors. With this approach, the size of a simulation box is only restricted by the number of cores and processing power of the computer being used. For these simulations the constants used are K_1 = 12, K_2 = 1, w = 7 in Eq. 2, β_ρ = 10, β_η = 3.75 in Eq. 1, L = 10 in Eq. 5, and in Eq. 4 D_{surf} = 45, D_{gb} = 4.1, D_{vol} = 0.08. The values listed are temperature dependent simulation constants. Initial constants used for the simulation were gotten from [15]. These constants correspond to a ratio of surface to grain boundary diffusion which is approximately 10:1 and surface energy to grain boundary energy which is approximately 2:1. The ratio of energies was gotten from Equations 3 and 4 by plugging in the value of the constants listed above. The value for density in vapor phase (ρ_{vap}) was taken to be 0.000000089 and in solid phase (ρ_{sol}) was taken to be 0.9998. The microstructures in the simulation were initialized by setting the pixels inside a particle to the value of ρ_{sol} and the pixels in the vapor were given random values within 1 millionth of the value of ρ_{vap}. The simulation starts with the particles in contact.

The simulation beds for the larger particle bed simulations were set up using a particle bed generation simulation that generates particles to match an actual physical bed. The powder bed consists of spherical nanoparticles that are generated by defining a position and radius using DEM in a multiphase computational fluid dynamics, MFIX. Particle packings are generated using the MFIX-DEM discrete mass inlet function with each particle interacting with its neighboring particles. The particles are initially distributed randomly within the powder bed domain and are given an initial velocity and an initial set of boundary conditions. The particles are subject to forces such as gravitational and cohesive forces. The particle interactions are modeled using a spring-

dashpot model based on a soft-sphere model of the particles. Under these forces, the particles are allowed to move around and interact until they reach a final steady state position, which creates the particle packing within the final powder bed used as an input for the PFM simulation [21].

Results and Discussion

Experimental sintering of nanoparticles

Copper nanoparticles were sintered using continuous wave lasers and the results are shown in the images below. The sintering experiments were conducted by spin-coating a layer of copper nanoparticle ink onto a flat substrate and drying the substrate to evaporate the solvent, leaving only a layer of copper nanoparticles. This layer of copper nanoparticles was then subjected to sintering underneath a continuous wave laser. Figure 1 shows the Scanning Electron Microscope (SEM) images of the copper nanoparticles before and after sintering occurs.

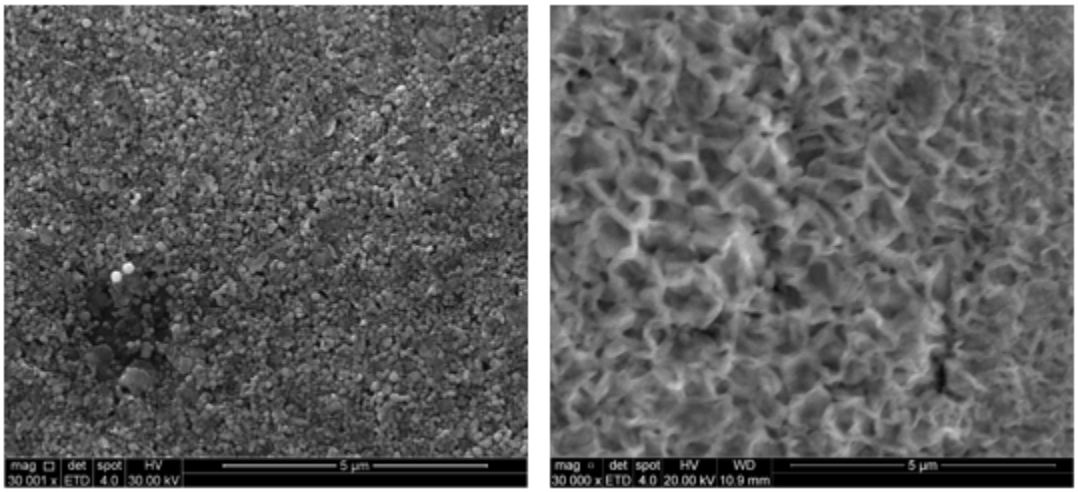

Figure 1. Sintering of copper nanoparticles. a) Unsintered. b) After sintering with a laser at 40mW and an exposure time of 500ms

The SEM images in Figure 1a show the granular layer of copper nanoparticles with separate particles. After sintering occurs, the particles form bonds diffusing into each other to form linkages that connect the previously separate particles to a single connected unit, visible in Figure 1b. This diffusion and coalescence of particles together during sintering can be compared to the results of the simulations of the beds discussed in further detail in the following sections.

2 particles of unequal size

In order to examine the effect of particle size on sintering kinetics, the PFM simulation was run first in a box of 40 by 40 by 40 voxels with two particles of unequal size. For this simulation, the bigger particle was set to have a diameter of 20 pixels and the smaller particle a diameter of 10 pixels. The results are shown in Figure 2.

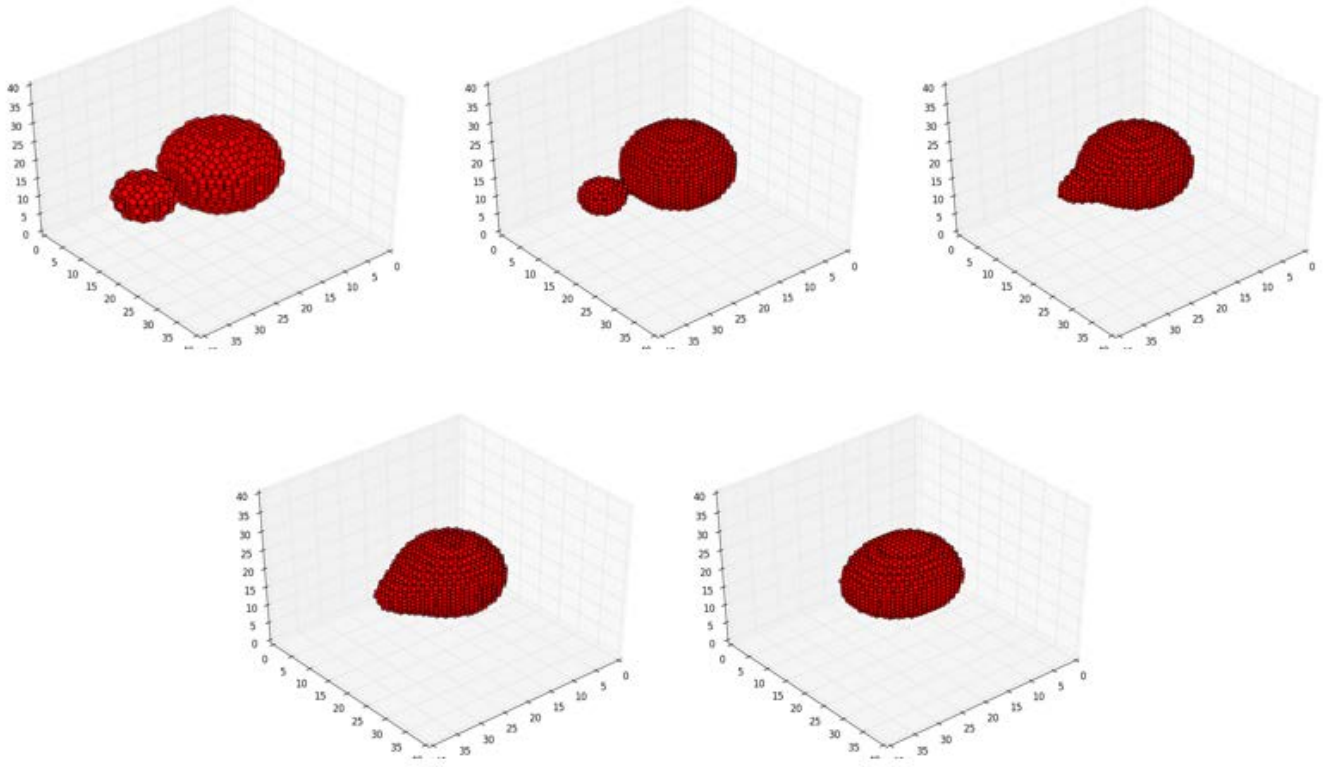

Figure 2. The evolution of two particles with unequal sizes during sintering. a) Initial b) 2500 time steps c) 12500 time steps d) 22500 time steps e) 50000 time steps

At the start of the process the particles are just touching to initiate diffusion. As sintering progresses a neck starts to form between particles which continues to grow until the onset of coarsening. During the process of coarsening, the boundary between the particles migrates into the smaller particle shifting the mass balance towards the bigger particle. As the simulation time increases, this shrinkage continues until only a single spherical particle remains at steady state. At 50,000 time steps the simulation is approaching steady state but has not quite reached it. The initial sintering periods are characterized by fast neck growth between particles which slows down as coarsening begins. The two particle simulation took 7.2 minutes to run to the final timestep using a single processor. This length of time for two particles running to 50,000 time steps shows the need for parallel computing to achieve higher final times with larger size beds and higher number of particles.

1 by 1 micrometer bed

In order to test larger particle beds, the two particle simulation procedure was expanded using MPI to handle a large bed characteristic of an actual μ-SLS process. The bed shown in Figure 3, has 43 particles in a simulation box with dimensions of 110 pixels by 110 pixels in the x-y plane and 73 pixels in the z. As discussed earlier, this simulation bed was produced using a powder bed model that randomly places the nanoparticles in a fixed domain with random initial velocity vectors and lets the nanoparticles settle into a steady state powder bed using various dissipation mechanisms. The particle interactions in this simulation are governed mainly by gravitational forces [21]. The steady state arrangement of these particles are then imported into the PFM simulation. The bed used for the one by one micrometer study had a maximum height of 687 nm

and was made up of particles with diameters ranging from 73 to 287 nm. The pixel conversion factor used for converting the sizes in nanometer length to pixels was 0.00882 nm/pixel. The results from the simulation of the one by one micron bed are shown in Figure 3.

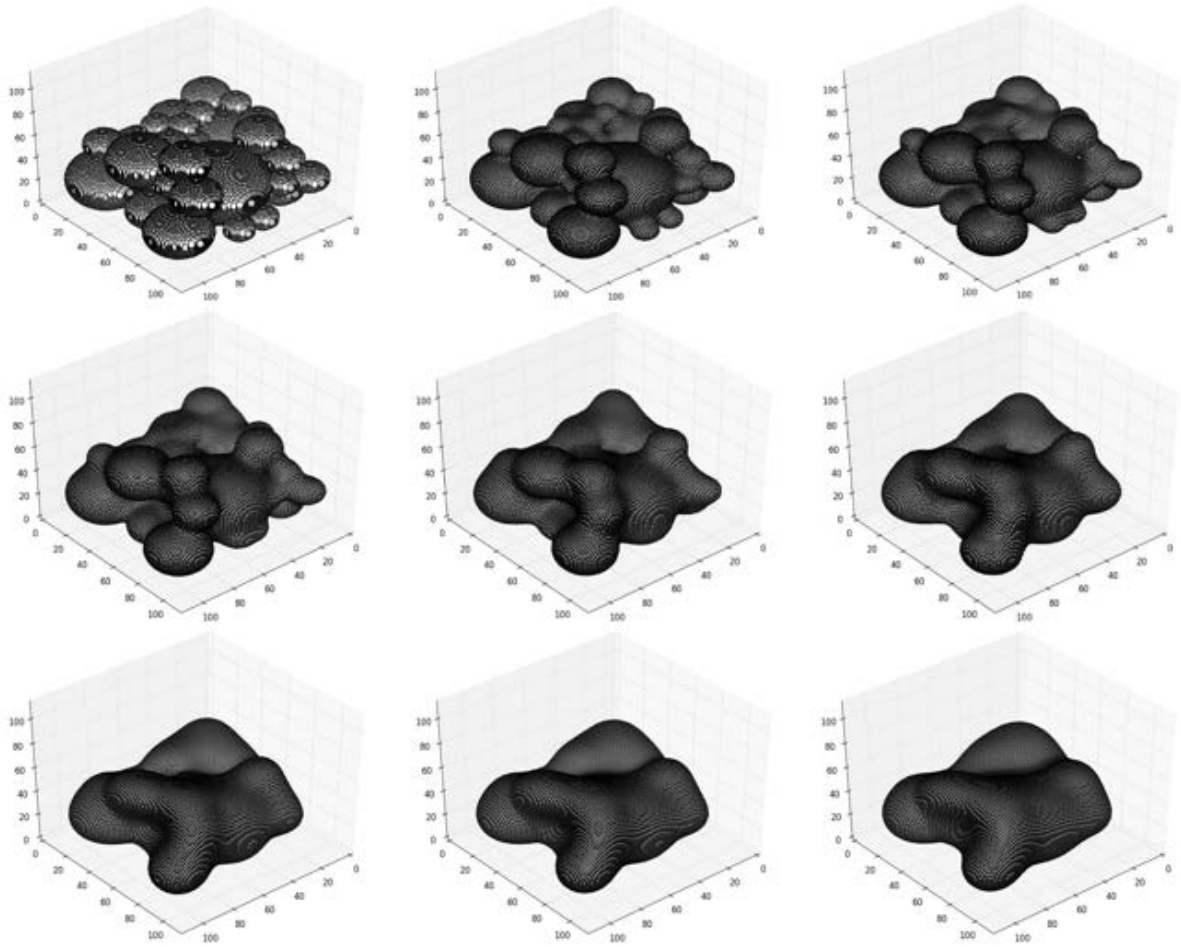

Figure 3. The evolution of a one by one micrometer bed with 43 particles. a) Initial b) 20000 time steps c) 60000 time steps d) 100000 time steps e) 280000 time steps f) 450000 time steps g)700000 time steps h) 850000 time steps i) 1100000 time steps

The images in Figure 3 follow a similar trend to the 2 particle simulation shown in Figure 2. At the initial time steps (3a-d) the neck formation happens rapidly leading to a faster looking rate of evolution than in the later time steps. The shrinkage and densification is, however, clear in the later images (3f-i) as the pores prevalent in previous time steps are filled due to the diffusion between particles as sintering occurs. The simulation of the bed shown in Figure 3 was modeled under isothermal conditions with each particle having the same diffusion constants.

Analysis was done on the simulation above to calculate the change in height of the particle bed with time as well as the change in density. From the images in Figure 3, it is clear that there is shrinkage along the x and y axis as well as the z. This is due to the simulation environment

modeling sintering of a particle bed surrounded by pixels in the vapor phase. To accurately analyze the data from the simulation the results were obtained by analyzing the trends inside a 40 by 40 pixel box in the center of the bed, which corresponds to a 423 by 423 nm box. Doing the simulation in the center makes the analysis impervious to the x-y shrinkage occurring at the edges. The relative density in the analysis box was calculated by taking the ratio of the sum of density variables of the porous box to that of a completely filled box. Therefore, the relative density is at its minimum at the start of the simulation and density increases during the simulation as the nanoparticles start to sinter together and reduce the porosity of the bed. At the end of sintering the relative density approaches a maximum as shrinkage occurs so that the bed reaches steady state when the pixels completely fill the analysis box. The results for the relative density and maximum height from the one by one micron bed are shown in the images below.

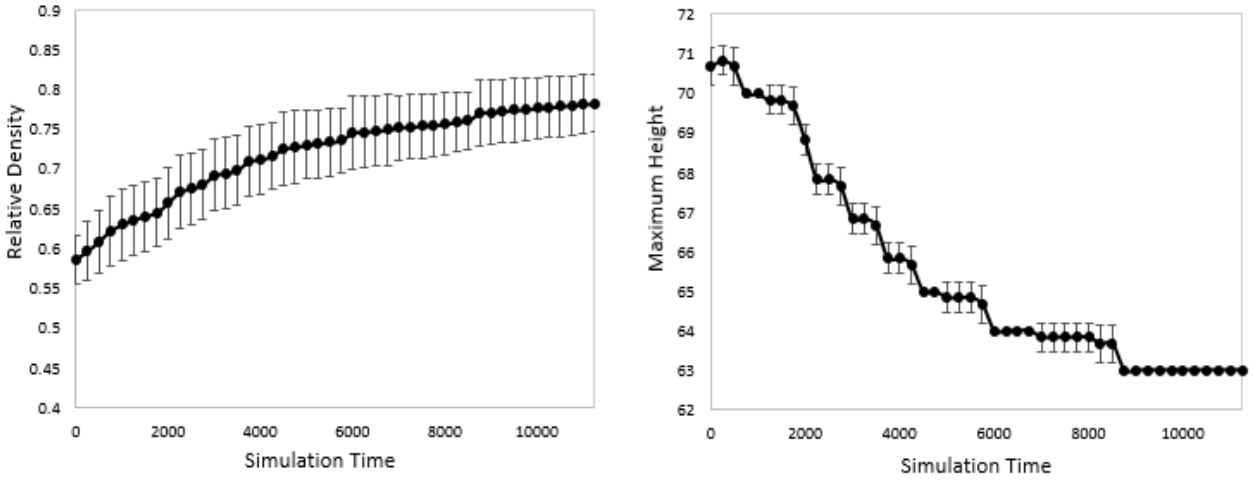

Figure 4. Analysis of the density and height change in the sintering of a one by one micrometer bed. a) Relative Density b) Maximum Height change

The results in Figure 4 show that the simulation process follows the expected trend with increasing density and decreasing height over time. The error bars in Figure 4 were gotten from changing the location of the pixel analysis box in the middle of the simulation. These errors represent the variability inherent in the location where the analysis is carried out. Data analysis shown in Figure 4 was compared against experimental data gotten from the sintering of beryllium oxide nanoparticles [22] which is shown in Figure 5. The time on the x-axis was normalized to match the experimental data. The results in the plot show that the relative density data gotten from literature falls within the error bounds of the simulation results. Figure 5 highlights the viability of obtaining data from the simulation which can be compared to experimental data.

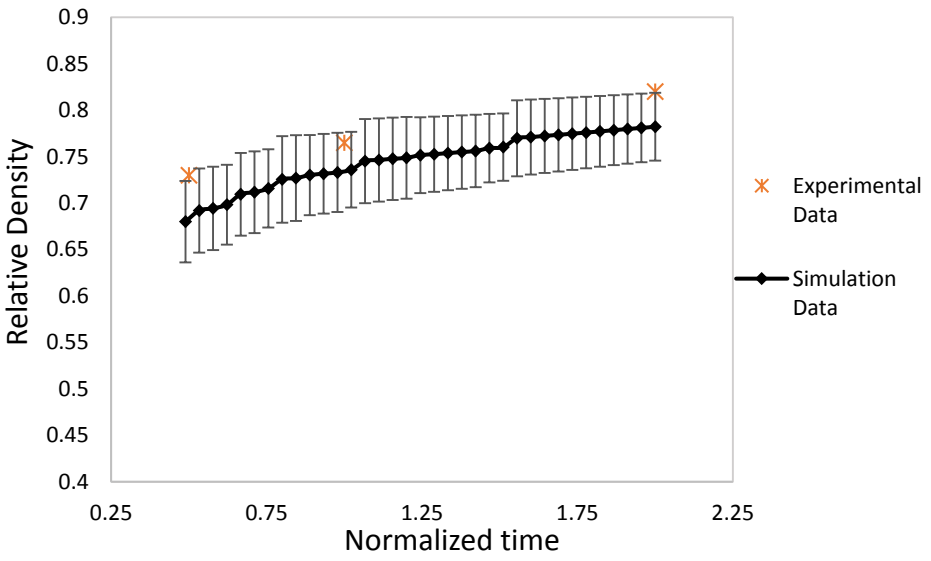

Figure 5. Comparing relative density results for the sintering of nanoparticles between simulation data and experimental data

2 by 2 micrometer bed

Using a similar analysis as on the one by one micron bed, the simulation was tested on a two by two micron bed containing 134 particles. As was the case with the smaller bed the simulation bed was produced using the random computer generation of particles mirroring an actual experiment. This bed had particles with diameters ranging from 118 to 572 nm, which was converted to a simulation bed with dimensions of 286 pixels by 282 pixels in the x y plane and 98 pixels in the z. The results from the simulation are shown in Figure 6.

The 134 particle system on the 2 by 2 micrometer bed highlighted the capabilities of the PFM model run with MPI libraries. On an initial run of the system using 140 processors, the simulation ran to 220,000 simulation time steps in 48 hours. The simulation was next run with 960 processors which was able to reach 500,000 time steps in 16.5 hours. Following this trend, the simulation can reach even higher time steps when run with larger number of processors.

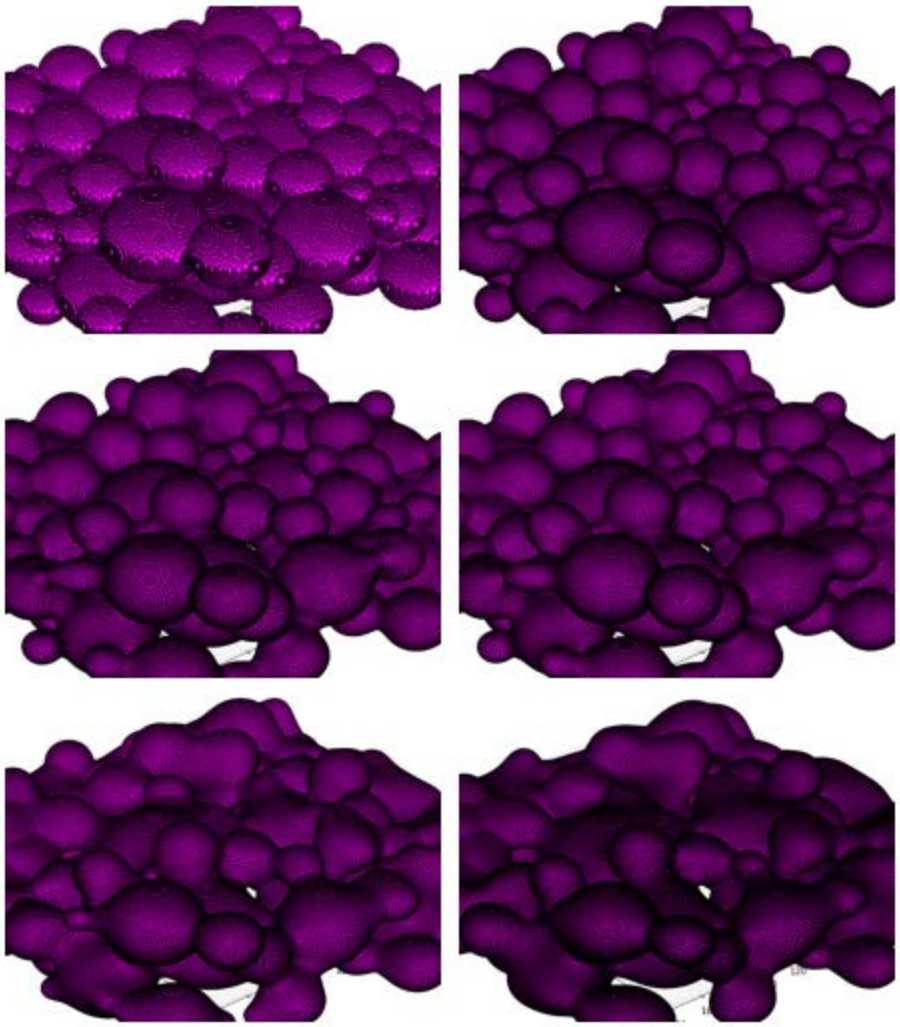

Fig 6. The evolution of a two by two micrometer bed with 134 particles. a) Initial b) 20000 time steps c) 60000 time steps d) 100000 time steps e) 280000 time steps f) 500000 time steps

Future Work

It is important to keep in mind that the constants used for the analysis in the Results section were kept constant throughout the simulation. As discussed in the previous sections, each of these constants are related to either the surface or grain boundary energy or the diffusion in the system. Diffusion coefficients and energy measurements are dependent on the temperature of the bed. For a typical SLS process, this temperature measurement will vary based on the laser position on the bed. As such, to accurately model the process, the constants used for the simulation have to be calibrated to match actual physical temperatures. This calibration can be done by measuring the shrinkage and density changes for a physical sintering experiment at different time points and comparing the simulation analysis results, curve shown in Figure 4, against the analysis of the experimental results.

Another important parameter that needs to be considered in order to accurately model the μ-SLS process is to track the path of the laser acting on the system and have differential heating (sintering) based on the location of the laser on the bed. This modification to the simulation will be the next step after the simulation parameters are determined from the calibration of the simulation results against experimental data. Another future modification would be to expand the simulation to have more than one layer so that the interactions between layers can be studied as to their effect on the final manufactured part.

Conclusion

In this paper, a Phase Field Modelling approach has been demonstrated to simulate the sintering of particles in a powder bed. Making use of Parallel programming through MPI, this study shows the validity of using PFM to model sintering of nanoparticles starting with a small bed with 43 particles to a large bed made up of 134 particles. The approach described here was able to reduce the run time by a factor of three to get to double the final simulation time. Data analysis was also carried out on the 43 particle bed simulation which shows expected density and shrinkage trends. The results from this study will be compared to experimental results for nanoparticle shrinkage in order to determine the exact grain boundary and surface diffusion coefficients of the nanoparticle systems being studied.

Acknowledgements

This study was made possible through the Supercomputing resources of the Texas Advanced Computing Center. The authors would also like to thank NXP Semiconductors for the financial support provided.

References

[1] “Design Guidelines: Laser Sintering (LS).” (n.d.). Retrieved June 28, 2017, from https://www.stratasysdirect.com/resources/laser-sintering/.

[2] Sager, B., and Rosen, D., (n.d.), “Stereolithography Process Resolution,” Georgina Institute of Technology.

[3] Roy, N. K., Foong, C. S., and Cullinan, M. A., 2016, “Design of a Micro-scale Selective Laser Sintering System,” 2016 Annual International Solid Freeform Fabrication Symposium.

[4] Roy, N., Yuksel, A., and Cullinan, M., 2016, “Design and Modeling of a Microscale Selective Laser Sintering System,” ASME 2016 11th International Manufacturing Science and Engineering Conference.

[5] Roy, N., Dibua, O., Foong, C. S., and Cullinan, M., 2017, “Preliminary Results on the Fabrication of Interconnect Structures Using Microscale Selective Laser Sintering,” Proceedings of the ASME 2017 International Technical Conference and Exhibition on Packaging and Integration of Electronic and Photonic Microsystems.

[6] Dong, L., Makradi, A., Ahzi, S., and Remond, Y., 2009, “Three-dimensional transient finite element analysis of the selective laser sintering process,” Journal of Materials Processing Technology, **209**, pp. 700-706.

[7] Moser, D., Cullinan, M., and Murthy, J., 2016, “Particle-Scale Melt Modeling of the Selective Laser Melting Process,” 2016 Annual International Solid Freeform Fabrication Symposium, pp. 247-256.
[8] Moser, D., Fish, S., Beaman, J., and Murthy, J., 2014, “Multi-Layer Computational Modeling of Selective Laser Sintering Processes,” ASME 2014 International Mechanical Engineering Congress and Exposition, **2A**, pp. V02AT02A008- V02AT02A018.
[9] Ko, S. H., and Grigoropoulos, C. P., 2008, “The Solid-State Neck Growth Mechanisms in Low Energy Laser Sintering of Gold Nanoparticles: A Molecular Dynamics Simulation Study,” Journal of Heat Transfer, **130**, pp. 092404-1 – 092404-7.
[10] Rojek, J., Nosewicz, S., Pietrzak, K., Chmielewski, and M., Kalinski, D., 2011, “Modelling of powder sintering using the discrete element method,” Computer Methods in Mechanics.
[11] Ding, L., Davidchack, L. R., and Pan, J., 2009, “A molecular dynamics study of sintering between nanoparticles,” Computational Materials Science, **45**, pp. 247-256.
[12] Cheng, B., and Ngan, H. W. A., 2013, “The Sintering and Densification Behavior of Many Copper Nanoparticles: A molecular Dynamics Study,” Computational Materials Science, **74**, pp. 1-11.
[13] Shinagawa, K., 2014, “Simulation of Grain Growth and Sintering Process by Combined Phase-Field/Discrete Element Method,” Acta Materialia, **66**, pp.360-369.
[14] Wang, U. Y., 2006, “Computer Modeling and Simulation of Solid-State Sintering: A Phase Field Approach,” Acta Materialia, **54**, pp. 953-961.
[15] Kumar, V., 2011, “Simulations and modeling of unequal sized particles sintering,” Diss. The University of Utah.
[16] Moelans, N., Blanpain, B., and Wollants, P., 2008, “An introduction to phase-field modeling of microstructure evolution,” Computer Coupling of Phase Diagrams and Thermochemistry, **32**, pp. 268-294.
[17] Chockalingam, K., Kouznetsova, V. G., van der Sluis, O., and Geers, M. G. D., 2016, “2D Phase field modeling of sintering of silver nanoparticles,” Comput. Methods Appl. Mech. Engrg.
[18] Cahn, J. W., and Hilliard, J. E., 1958, “Free Energy of a Nonuniform System. I. Interfacial Free Energy,” The Journal of Chemical Physics, **28**, pp. 258-267.
[19] Cahn, J. W., 1961, “On Spinodal Decomposition,” Acta Metallurgica, **9**, pp. 81-87.
[20] Ginzburgh, V. L., andLandau, L. D., 1950, “On the theory of superconductivity,” Soviet Physics – Journal of experimental and Theoretical Physics, **20**, pp. 1064-1082
[21] Yuksel, A., and Cullinan, M., 2016, “Modeling of nanoparticle agglomeration and powder bed formation in microscale selective laser sintering systems,” Additive Manufacturing, **12**, pp. 204-215.
[22] Wang, X., Wang, R., Peng, C., Li, T., and Liu, B., 2010, “Synthesis and sintering of beryllium oxide nanoparticles,” Progress in Natural Science: Materials International, **20**, pp. 81-86.